Optical second harmonic generation in LiB3O5 modulated by intense femtosecond X-ray pulses

Journal Article

Author(s):
Deng, Yunpei; Zerdane, Serhane; Xie, Xinhua; Divall, Edwin; Johnson, Philip J.M.; Arrell, Christopher; Lemke, Henrik T.; Mankowsky, Roman; Oggenfuss, Alex; Svetina, Cristian; Erny, Christian; Cirelli, Claudio; Milne, Christopher; Knopp, Gregor; Beaud, Paul; Johnson, Steven L.

Optical second harmonic generation in LiB$_3$O$_5$ modulated by intense femtosecond X-ray pulses

Yunpei Deng,[1,*] Serhane Zerdane,[1] Xinhua Xie,[1] Edwin Divall,[1] Philip J. M. Johnson,[1] Christopher Arrell,[1] Henrik Till Lemke,[1] Roman Mankowsky,[1] Alex Oggenfuss,[1] Cristian Svetina,[1] Christian Erny,[1] Claudio Cirelli,[1] Christopher Milne,[1] Gregor Knopp,[1] Paul Beaud,[1] and Steven L. Johnson[1,2]

[1]*SwissFEL, Paul Scherrer Institute, Villigen, Switzerland*
[2]*Institute for Quantum Electronics, Physics Department, ETH Zurich, Zurich, Switzerland*
*yunpei.deng@psi.ch

Abstract: Many of the scientific applications for X-ray free-electron lasers seek to exploit the ultrashort pulse durations of intense X-rays to obtain femtosecond time resolution of various processes in a "pump-probe" scheme. One of the limiting factors for such experiments is the timing jitter between the X-rays and ultrashort pulses from more conventional lasers operating at near-optical wavelengths. In this work, we investigate the potential of using X-ray-induced changes in the optical second harmonic generation efficiency of a nonlinear crystal to retrieve single-shot arrival times of X-ray pulses with respect to optical laser pulses. Our experimental results and simulations show changes to the efficiency of the second harmonic generation of 12%, approximately three times larger than the measured changes in the transmission of the 800 nm center-wavelength fundamental pulse. Further experiments showing even larger changes in the transmission of 400 nm center-wavelength pulses show that the mechanism of the second harmonic generation efficiency modulation is mainly the result of X-ray-induced changes in the linear absorption coefficients near 400 nm. We demonstrate and characterize a cross-correlation tool based on this effect in reference to a previously demonstrated method of X-ray/optical cross-correlation.

1. Introduction

X-ray free-electron lasers provide a powerful tool for investigating fundamental structures and dynamics of materials in physics, chemistry, and biology [1–5]. One significant advantage of X-rays from free-electron lasers is the ability to create pulses with a very short duration compared to typical picosecond-duration pulses from third-generation synchrotron radiation sources. This development allows both structural and electron dynamics to be followed on a femtosecond time scale. Since the majority of pump-probe experiments currently conducted at X-ray free-electron lasers use femtosecond pulses from optical-wavelength lasers in combination with the X-ray pulses, the temporal resolution is typically determined not only by the pulse durations of the X-ray and optical pulses but also by the timing jitter between them. Although significant efforts have been undertaken to improve the synchronization between the FEL and laser systems [6,7], it is a challenge to limit the timing jitter to levels below a few tens of femtoseconds.

One widely adopted solution to obtain time resolution below the jitter limit is to measure directly the single-shot arrival times of X-ray pulses with respect to pulses from the laser during a pump-probe measurement. There are several different approaches to this that have been demonstrated [7–16]. One such method involves using the external laser to generate THz pulses, which then modulate the energy of photoelectrons liberated from a gas by the absorption of X-ray

photons [7,12,17]. This method is capable of measuring the X-ray pulse duration in addition to the arrival time but requires intense probe pulses at THz frequencies combined with a relatively complex detection system housed in a vacuum chamber. Another method involves using the X-rays to modulate the optical properties of a solid-state material on femtosecond time scales and then measuring these changes via the reflectivity or transmission of ultrashort pulses derived from the external laser system [8–11]. This is typically accomplished by using the X-rays to produce a large number of electron-hole pairs in a semiconducting or insulating material, which modulates the refractive index [18,19]. In order to measure these changes over a long time interval using only a single probe pulse, the interaction time of the probe is extended either by introducing spectral chirp to the probe or by introducing a large angle between the X-ray pump and laser probe. When using chirped laser pulses as a probe, time-dependent changes in transmission can then be probed with the measured spectrum from the linear relationship between time and wavelength. Alternatively, the use of a large angle between the pump and probe gives a strong correlation between pump-probe delay and position along one spatial direction. The probe light transmitted or reflected from the interaction region is then imaged onto a camera. Since the position along one direction along the camera is linearly correlated to the pump-probe delay, the modulation of the probe along this direction gives a direct measure of the time-dependent changes in the optical properties in this so-called "spatial timing tool." Both spectral- and spatial-encoding methods generally suffer from the drawback that in order to obtain high sensitivities, a large number of X-ray photons must be absorbed by the solid target. This, in turn, limits the X-rays available for the actual experiment. This has led to considerable interest in optimizing the optical sensitivity of such tools, so as to minimize these absorption losses for the X-rays.

Current realizations of this concept of solid-state single-shot timing diagnostics are all based on X-ray induced changes in the linear susceptibility. In optical spectroscopy, however, nonlinear processes often offer enhanced sensitivity to small perturbations, and in some cases can provide nearly background-free signals. Here we investigate the potential of using a prototype $\chi^{(2)}$ process, second harmonic generation, to measure the X-ray induced changes and to explore its potential usefulness as an X-ray timing diagnostic.

In this work we performed measurements and theoretical simulations on the X-ray-induced changes of second harmonic generation (SHG) from a single crystal of LiB_3O_5 (LBO). In the experiment, we perform pump-probe measurements where hard X-rays excite the LBO and the changes in optical properties are probed by monitoring the efficiency of second harmonic generation from a femtosecond pulse with a center wavelength of 800 nm. These changes in efficiency can in principle arise from several different physical processes, including (i) X-ray induced changes of the second-order nonlinear susceptibility $\chi^{(2)}$; (ii) X-ray induced changes in the real part of the index of refraction n for either the fundamental or second harmonic wavelengths (thus modulating the phase matching condition); or (iii) X-ray induced changes in the imaginary part of the index of refraction k for either the fundamental or second harmonic wavelengths. Our results reveal that changes in neither the second-order susceptibility $\chi^{(2)}$ nor the phase-matching play a major role in the observed modulation of SHG signals in LBO. They are rather dominated by the change in optical absorption induced by the X-rays in the LBO crystal at fluences below 150 mJ/cm^2 at 7 keV photon energy. We support this conclusion with simulations employing a one-dimensional coupled-wave model.

2.   Experiment setup

The experiment was carried out in the Bernina endstation at the SwissFEL Aramis hard X-ray beamline [20]. The Aramis beamline delivers X-ray pulses with photon energies up to 12 keV. In our experiment, the photon energy was tuned between 7 keV and 9 keV with a repetition rate of 50 Hz. The electron bunch was around 50 fs RMS. It was estimated to produce an X-ray pulse duration below 50 fs. A Ti:Sapphire femtosecond laser, electronically synchronized with the

free-electron laser, provides the optical probe pulses with a center wavelength of 800 nm and a fully compressed pulse duration of 30 fs [21]. Although the maximum pulse energy generally available for experiments is 10 mJ, only approximately 1 μJ was required for this experiment.

The experimental setup is shown in Fig. 1. The X-ray beam is focused by a pair of Kirkpatrick-Baez mirrors. The LBO crystal is placed into the converging beam which at this position has a spot size of 200 μm (FWHM). Using the beamline solid-state attenuator system (silicon and diamond filters) the X-ray pulse energy is attenuated to 170 μJ. The LBO crystal is 50 μm thick, with an X-ray transmission of approximately 85% at 7 keV. The entrance and exit surfaces of the LBO crystal are at 31.6 degrees from the optical axis in the XY principal axis plane to meet the type I SHG phase matching condition for 800 nm at normal incidence. To probe the optical response of the crystal, a lens focuses the 800 nm beam onto the crystal with a spot size of 100 μm, crossing the X-rays within the LBO at an angle of 0.8 degrees. We adjust the pulse energy of the 800 nm beam to keep the peak intensity below 10^{10} W/cm^2, where the SHG remains in the small-signal-gain regime. After the LBO, a grating spectrometer measures the transmitted probe spectrum, including the second harmonic generated by the LBO. The spectrometer covers the spectral range from 200 nm to 1100 nm with approximately 0.5 nm resolution. Since the fundamental 800 nm pulse is much more intense than the second harmonic, a 99.9% high reflection mirror for 800 nm is placed before the spectrometer entrance slit to attenuate the 800 nm pulses to avoid saturation of the detector in the spectrometer. The near-infrared laser pulses were temporally stretched to around 400 fs by detuning the grating compressor, resulting in a negative chirp that was used to encode the arrival time information spectrally on both the fundamental and SH signals. A linear delay stage in the 800 nm beam path controls the average arrival time relative to the X-rays. This delay stage is also used to calibrate the relationship between wavelength and arrival time for both the fundamental and SH pulses. In the measurements described in section 3, a total of 200 laser shots are recorded for each time step. The pump laser is operating at twice the repetition rate of the FEL pulses sampling alternately pumped and unpumped spectra for reference.
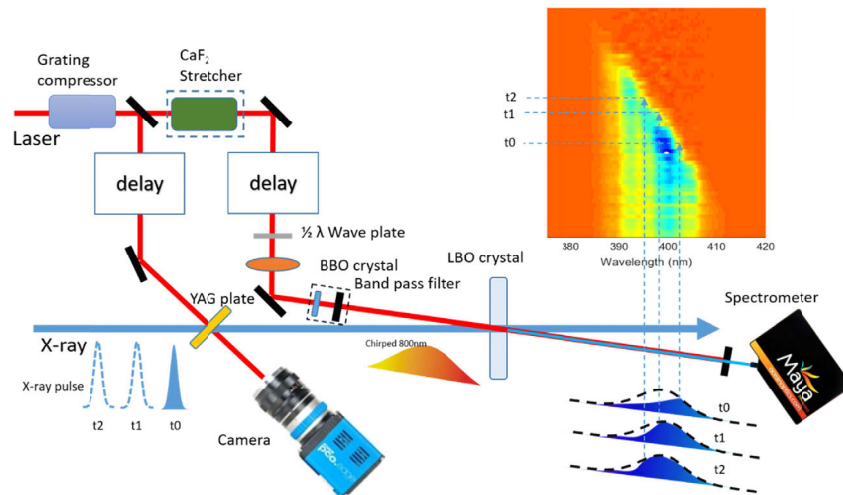
Fig. 1. Schematic view of the experimental setup. The BBO crystal and bandpass filter in the dashed frame are placed only for the 400 nm measurements and the 10 cm CaF$_2$ stretcher is placed only for correlation with spatial encoding. The Y$_3$Al$_5$O$_{12}$ (YAG) plate and the camera are used for the spatial encoding timing tool.

As is briefly discussed in the introduction, the second harmonic generation can be influenced by the absorption of X-rays in the LBO in several different ways. One such mechanism is an

X-ray-induced change in the linear absorption of the generated second harmonic pulses. To investigate this, we performed another set of experiments where a 50 μm-thick BBO crystal was inserted into the stretched 800 nm beam, generating pulses with a wavelength centered at 400 nm. A 400 nm bandpass filter removes the residual 800 nm before interaction with the LBO. Measurements are then conducted using the 400 nm pulses and varying the pump-probe delay. This allows us to measure the effect that X-ray excitation has on the time-dependent linear absorption coefficient of the 400 nm light.

We also performed benchmark comparisons of our SHG-based cross-correlator to a more conventional setup based on spatial-encoding of the time delay, which we will refer to as the "spatial timing tool" [7–9,16]. For the spatial timing tool, 30 fs compressed pulses are used, while for the SHG experiment the laser pulses are stretched to 200 fs by passing through a 10-cm rod of CaF$_2$. The results are described in Section 3.

3.   Results and discussions

3.1.   *X-ray induced changes in SHG*

#### 3.1.1.   Experimental results

Figures 2(a) and 2(b) show the spectra of the fundamental and SHG, respectively. The blue curves show the spectra without the X-ray pump. The red curves show the spectrum when the X-ray pulse overlaps with the chirped laser pulse. The arrival time information can be extracted by analysis of the difference between the pumped and unpumped data.
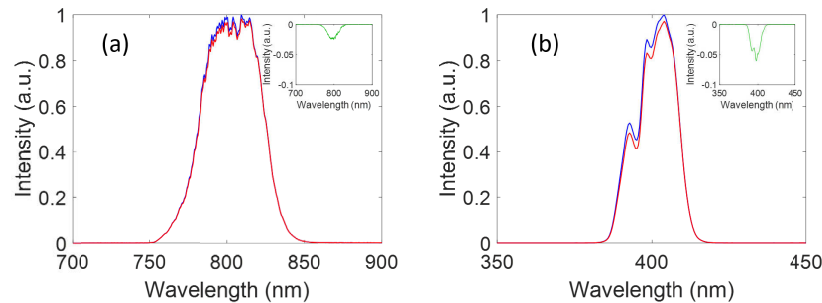
Fig. 2. Typical spectra of the transmitted probe through the LBO under optimized phase-matching conditions where the X-rays are blocked (blue) and where the X-rays are applied, overlapped in the middle of the laser pulse (red), in the vicinity of the fundamental (a) and second harmonic wavelengths (b). The spectra shown are normalized to their peak value. The residual of the fundamental is centered at 800 nm with a width of 44 nm (FWHM) and the second harmonic is peaked at 400 nm with a width of 16 nm (FWHM). The insets present the normalized difference between the corresponding spectral signals with and without X-rays.

Figure 3(a) shows the difference between the fundamental spectra measured with and without X-ray pulses versus the average pump-probe time delay as determined by the delay line stage position. Increasing values indicate that the optical pulses arrive later relative to the X-rays. The difference is normalized to the peak intensity without X-ray pulses. Figure 3(b) shows the same for the second harmonic spectra. The measurements clearly show X-ray-induced changes in both spectral ranges when the optical pulse arrives after the X-ray pulse. The onset time of the change depends on the wavelength, with shorter wavelengths requiring longer probe delays. This is an expected consequence of the negative chirp of the fundamental, which gives a linear relationship between the effective pump-probe delay and wavelength. For delay stage settings where the

optical pulse overlaps the X-ray pulse in time, the wavelength dependence of the intensity can be used to determine the arrival time of the X-rays on a per-shot basis.
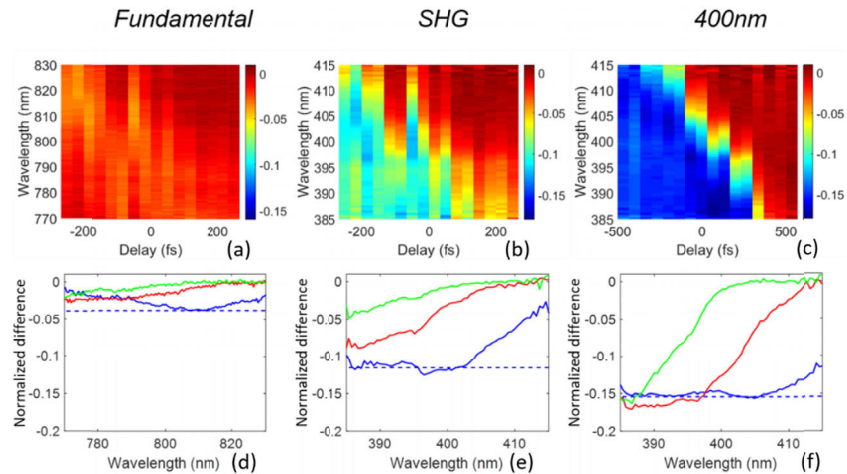

Fig. 3. Measured X-ray induced signal changes over wavelength and time delay between the X-ray pulse and the laser pulse for the fundamental (a), the SHG in the LBO crystal (b) and the pre-generated 400 nm measurement (c). Note that due to the somewhat larger chirp of the pre-generated 400 nm, the range and step size of the 400 nm measurement (c) is larger than that of the SHG measurement. Panels (d), (e) and (f) present the slices of (a), (b) and (c) at delays of 240 fs (green), 30 fs (red) and −180 fs (blue). The dashed lines are simulated signal differences in the spectrum of the fundamental (c), and the second harmonic generated in the LBO crystal (d) and 400 nm radiation generated separately in the BBO crystal before the absorption measurement (e) when the X-ray pulse overlaps the center of the chirped pulse for zero delay. A negative delay indicates that the X-ray pulse comes before the center of the external laser pulse.

To make a more direct comparison between the X-ray induced changes in the fundamental and second harmonic, we show in Figs. 3(d) and 3(e) plots of the difference spectra for pump-probe delays of 240 fs, 30 fs, and −180 fs. The spectra look quite similar, but the X-ray induced change in the second harmonic is approximately three times larger than that of the fundamental. This indicates that the second harmonic signal is significantly more sensitive to the X-ray-induced changes to the sample.

Figure 4(a) shows the SHG spectrum (without X-ray interaction) as a function of the angle of the LBO sample from the optical axis, rotated within the XY plane. Figure 4(b) shows the dependence of the difference between the X-ray pumped and unpumped signal as a function of wavelength and angle, at a delay of 200 fs and an X-ray fluence of 150 mJ/cm^2. The difference is almost identical in shape and position to the unpumped signal, which indicates that the phase-matching angle is not strongly modified by the X-ray pulse.

We also measured X-ray-induced changes to the transmission of compressed optical pulses at a center wavelength of 400 nm, generated before the sample. The spectral changes of this 400 nm pulse with the same X-ray excitation parameters are depicted in Fig. 3(c) as a color map, and in Fig. 3(f) as a line-out. The overall shape of the spectrum at these delay times is comparable to the spectrum at late delay times for the 800 nm pulses. We note, however, that the overall magnitude of the change is even larger for the pre-generated 400 nm than for the second harmonic signal from the LBO.
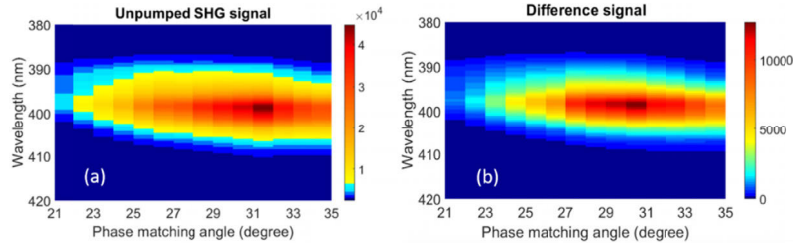
Fig. 4. (a) SHG spectrum as a function of phase matching angle, (b) the change of the pumped spectral signal with respect to the unpumped spectral signal as a function of the phase matching angle.

3.1.2. Simulations

To gain further insight into our experimental observations, we performed simulations using a coupled-wave model for SHG [22,23]. Guided by the experimental results, we model the X-ray induced changes as a sudden, step-like change in the linear absorption coefficients at the fundamental and second harmonic wavelengths. Let $A_{1,2}(z,t)$ be the amplitude of the electric field at a depth z and a time t for the fundamental and second harmonic beams, respectively. For times t after the X-ray pulse interaction, the coupled-wave theory then predicts that these amplitudes must satisfy

$$\frac{\partial A_1}{\partial z} = -\alpha_{FC1}A_1 - iv_{g1}\frac{\partial A_1}{\partial t} - i\beta_1\frac{\partial^2 A_1}{\partial t^2} - \frac{8\pi i\omega_1^2 d_{eff}}{k_1 c^2}A_2 A_1^* e^{-i(2k_1-k_2)z}$$

$$\frac{\partial A_2}{\partial z} = -\alpha_{FC2}A_2 - iv_{g2}\frac{\partial A_2}{\partial t} - i\beta_2\frac{\partial^2 A_2}{\partial t^2} - \frac{4\pi i\omega_2^2 d_{eff}}{k_2 c^2}A_1^2 e^{-i(2k_1-k_2)z}$$

$$\alpha_{FC1,2} = \frac{N\lambda_{1,2}^2 q^2}{4\pi^2\varepsilon_0 m_c c^3 n\tau} \tag{1}$$

where $A_{1,2}$, $\omega_{1,2}$, $v_{g1,2}$, $\beta_{1,2}$, $\lambda_{1,2}$ and $k_{1,2}$ are the electric field amplitudes, center frequencies, group velocities, group velocity dispersions, wavelengths and wave vectors of the fundamental and the second harmonic probe pulses. Here d_{eff} is the second-order nonlinear coefficient with a value of 0.749 pm/V for 800 nm SHG of LBO. The parameters α_{FC1} and α_{FC2} are the free carrier absorption coefficients of the fundamental and second harmonic wavelengths of light which originate from the X-ray generated electron-hole pairs [24]. q, ε_0, m_c, c, n, and τ are the fundamental charge, the vacuum permittivity, the conductivity effective mass of the free carrier, the speed of light, the real component of the refractive index and the mean time between collisions of the oscillating particles and the nuclei. N represents for the concentration of the free carriers which is proportional to the X-ray intensity in the crystal ($I_0 e^{-\gamma_x z}$) with γ_x the X-ray attenuation coefficient of LBO crystal. The free carrier absorption coefficient can be simplified into a form of $\alpha_{FC} = \alpha_0 e^{-\gamma_x z}$ with α_0 the free carrier absorption coefficient at the X-ray entrance point of the crystal ($z=0$). This formulation, Eq. (1), is valid only in the approximation that the X-ray induced changes occur before the optical probe interaction, and that the time-dependence of changes to the absorptions α_{FC1} and α_{FC2} are negligible over the time scale of the SHG interaction. To obtain the final spectra of the fundamental and the second harmonic pulse, we used the split-step method to propagate the pulses through the crystal with a step size of 0.5 µm.

In the simulations, we used the same X-ray and crystal parameters as those in the experiment. γ_x is obtained from the X-ray database for the absorption of 7 keV photons in LBO crystal, which is 6.6 cm^{-1} [25]. The free carrier absorption coefficients α_0 of 800 nm and 400 nm were

calculated to be $3\,\mathrm{cm}^{-1}$ and $9\,\mathrm{cm}^{-1}$ with the X-ray parameters of our experiments for LBO. Since we did not observe a clear modulation caused by the phase-matching condition in the experiment, the contribution due changes of the wave vectors is neglected in the simulation. For the simulation in the pre-generated 400 nm case, we considered the absorption by free electrons produced by X-rays as well.

The dashed line in Fig. 3(e) shows the simulated results of the signal change due to X-ray absorption. The differences are normalized to the spectral signal without X-ray absorption. In comparison with the experimental results in Fig. 3(e), the simulated results agree well with the experimental results. This suggests that the main contribution to the X-ray induced change in the second harmonic is an increase in the absorption coefficient at 400 nm. The simulations also show that the change in the 400 nm region of the spectrum is smaller for the SHG in the LBO crystal than for the pre-generated 400 nm pulse, in agreement with the experimental results. This is because the SHG in the LBO crystal was kept in the small-gain region, and the signal is therefore amplified as it moves through the crystal, as compared to the pre-generated case which only suffers absorption.

3.2.   Timing retrieval and correlation with the spatial encoding tool

In order to successfully apply this method to perform corrections for timing jitter, it is necessary to examine the transmitted spectra of the chirped pulses on a single-shot basis. The timing jitter of the X-rays relative to the external laser will cause small shifts in the spectrum that can then be read out. As a benchmark, we compare these single-shot measurements of the relative timing to the spatial timing tool discussed in Section 2 and sketched in Fig. 1. For the spatial timing tool, a 500 µJ X-ray beam with a photon energy of 8 keV and beam diameter $(1/e^2)$ of 600 µm was transmitted through a 20 µm thickness YAG plate at an angle of 45°. A 30 fs, 800-nm pulse derived from the Ti:Sapphire laser enters at normal incidence to the YAG plate, overlapping both spatially and temporally with the X-ray beam. The transmitted 800-nm beam at the exit is captured by a CCD camera. For the SHG measurements, the 800 nm pulse was chirped to 200 fs via transmission through a 10-cm CaF_2 rod, while maintaining a spectral bandwidth of 35 nm.

We used the X-ray-induced signal change in SHG for the spectral timing signal. Typical single-shot signals from both the SHG and the spatial timing tool are plotted in Fig. 5. In order to extract a value for the X-ray pulse arrival time from the SHG spectrum, each single-shot spectrum is first sent through a digital low pass filter which removes contributions from frequencies higher than 0.1π/pixel using a minimum-order filter with a stopband attenuation of 60 dB. The arrival time of the X-rays is then identified with the pixel value on the spectrometer detector that gives the time when the pump-probe effect first reaches half its maximum amplitude, which is always at higher pixel values than the position of maximum effect because of the negative chirp.

The spatial timing tool data is analyzed in a similar way. The binned camera images are first sent through the same digital low-pass filter for the spectral timing tool. The filtered data is then differentiated with respect to the pixel position. The position of the maximum of the derivative is then taken as the arrival time (in pixels) of the X-rays.

To determine the relation between the arrival time and the pixel position extracted from each of the two methods, we performed calibration measurements for the two timing tools by scanning the delay between the X-ray pulse and the laser pulse with two independent delay stages. The measured signals are averaged for 200 shots at each delay point. According to the calibration measurements, one pixel in the spatial encoding signal corresponded to 1.2 fs, while the SHG spectral encoding signal is 10.8 fs per pixel.
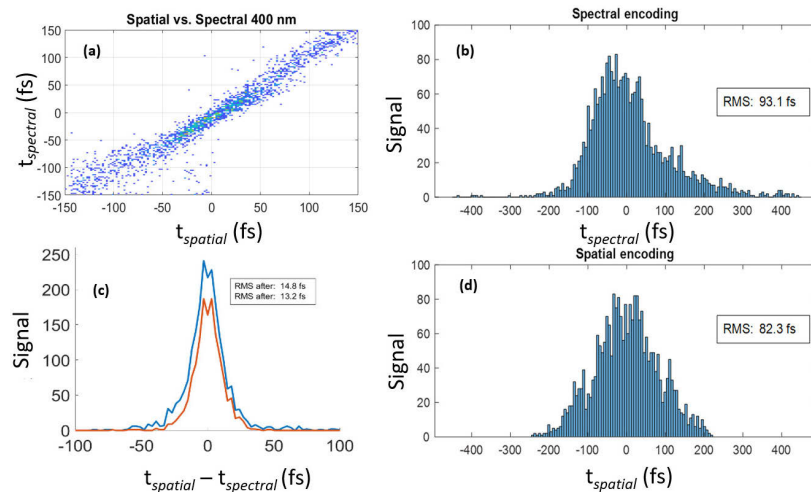
The correlation between the retrieved arrival time from the spatial timing tool and SHG spectral timing tool over 2500 shots is shown in Fig. 6(a). A clear correlation between the two timing techniques confirms that the changes in the SHG spectrum can serve as a timing diagnostic for single-shot timing corrections. The SHG spectral encoding and spatial encoding methods give
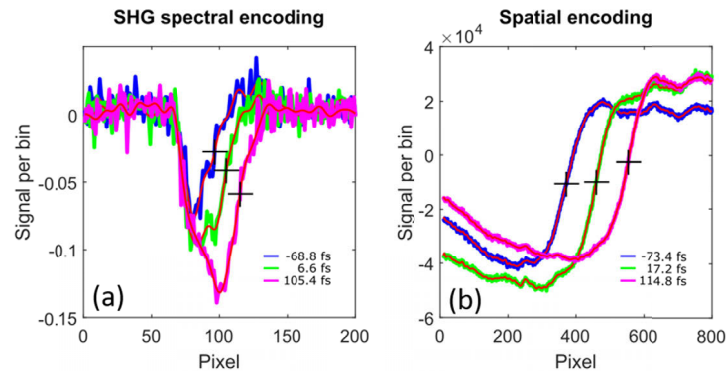
Fig. 5. Measured SHG spectral encoding (a) and spatial encoding (b) signals. The different colors show single-shot data for three different delays between the X-ray and optical laser with retrieved delays in the line legends. The thin red lines represent the data after applying a low pass filter. The time axis calibration are (a) 10.8 fs/pixel and (b) 1.2 fs/pixel, respectively.

estimates of the timing jitter between the laser and FEL of 80 to 90 fs RMS, respectively, as shown in Figs. 6(b)–6(d).

Fig. 6. (a) Measured the correlation between the SHG spectrum encoding and spatial encoding. (b) and (d) present the distributions of the arrival time measured with the SHG spectral timing tool and the spatial timing tool, respectively. (c) The distributions of the difference in the retrieved arrival time between the two timing tools (blue: all signal; red: signals in the timing jitter window from −50 fs to 100 fs).

The measurement time window of the spectral encoding is about 200 fs, which is slightly smaller than the overall jitter range. In order to evaluate the performance of the spectral encoding tool in comparison to the spatial timing tool, in Fig. 6(c) we show a histogram of the difference between the single-shot timing values for each shot. The width of this distribution gives a measure of the overall timing error for both methods. The blue curve shows the histogram where we consider data from across the entire range of the spectral encoding timing window and gives an RMS width of 14.8 fs. If we instead restrict the range of considered shots to those showing the onset of the X-ray induced changes at wavelengths with the largest signals (from −50 fs to

100 fs) the RMS width becomes 13.2 fs, which is slightly improved. Typically in SwissFEL, the timing jitter between the FEL pulse and the laser pulse is around 30-40 fs RMS. The temporal resolution of the SHG spectral encoding could be improved further with a spectrometer with better spectral resolution or with broader bandwidth laser pulses.

4. Discussion

Our results demonstrate the implementation of a method to use X-ray induced changes to SHG efficiency to measure on a single-shot basis the arrival time of hard X-rays from an FEL with a precision of approximately 15 fs, comparable in performance to methods based on X-ray induced changes in transmission or reflectivity of solid-state materials. The maximum X-ray induced change in the SHG efficiency in LBO at the wavelengths we used was approximately 12%. We also demonstrated by comparison with simulations that the mechanism for these X-ray induced SHG changes in LBO for 800 nm incident pulses is determined predominantly by changes in the linear optical absorption at the wavelength of the second harmonic. This was confirmed by X-ray pump, 400 nm probe experiments that show an even larger X-ray induced change in the transmission of 400 nm than is seen in the SHG efficiency, suggesting that a cross-correlator based on measuring changes in the transmission of 400 nm pulses would be in fact a more sensitive measurement of the arrival time in this particular case. There is to our knowledge no prior experimental study of the probe wavelength dependence of transmission-based cross correlators for X-rays, and our result suggests that further exploration of this is a promising route to increase sensitivity for this type of timing diagnostic. The reason for the enhanced sensitivity at 400 nm appears to contradict the predictions of a simple model of the excited crystal as a Drude metal [26,27], which would yield smaller effects at shorter wavelengths. The enhancement of the transmission change in this case may be due to the band structure of LBO: 3 eV photons have energy closer to the 7.78 eV bandgap of LBO, and is therefore more sensitive to changes in the occupation of valence and conduction band electrons redistributed by the X-rays. This would suggest that the optimization of the photon energy relative to the band gap could be an important control parameter.

In order to design an SHG-based timing diagnostic with clear advantages over a scheme based on X-ray driven changes to linear optical properties, much stronger modulation of the phase matching conditions and/or nonlinear susceptibility is required. One possibility for improvements is to narrow further the difference between the optical photon energy of the generated second harmonic with the optical bandgap of the SHG crystal. This should act to enhance possible X-ray induced changes in phase matching and/or $\chi^{(2)}$, potentially leading to nearly background-free cross correlation signals that will allow for wider timing windows and higher measurement precisions.

Acknowledgments

Disclosures

The authors declare no conflicts of interest.

References

1. C. Dornes, Y. Acremann, M. Savoini, M. Kubli, M. J. Neugebauer, E. Abreu, L. Huber, G. Lantz, C. A. F. Vaz, H. Lemke, E. M. Bothschafter, M. Porer, V. Esposito, L. Rettig, M. Buzzi, A. Alberca, Y. W. Windsor, P. Beaud, U.

Staub, D. Zhu, S. Song, J. M. Glownia, and S. L. Johnson, "The ultrafast Einstein–de Haas effect," Nature **565**(7738), 209–212 (2019).

2. W. Zhang, R. Alonso-Mori, U. Bergmann, C. Bressler, M. Chollet, A. Galler, W. Gawelda, R. G. Hadt, R. W. Hartsock, T. Kroll, K. S. Kjær, K. Kubiček, H. T. Lemke, H. W. Liang, D. A. Meyer, M. M. Nielsen, C. Purser, J. S. Robinson, E. I. Solomon, Z. Sun, D. Sokaras, T. B. van Driel, G. Vankó, T.-C. Weng, D. Zhu, and K. J. Gaffney, "Tracking excited-state charge and spin dynamics in iron coordination complexes," Nature **509**(7500), 345–348 (2014).

3. P. Nogly, T. Weinert, D. James, S. Carbajo, D. Ozerov, A. Furrer, D. Gashi, V. Borin, P. Skopintsev, K. Jaeger, K. Nass, P. Båth, R. Bosman, J. Koglin, M. Seaberg, T. Lane, D. Kekilli, S. Brünle, T. Tanaka, W. Wu, C. Milne, T. White, A. Barty, U. Weierstall, V. Panneels, E. Nango, S. Iwata, M. Hunter, I. Schapiro, G. Schertler, R. Neutze, and J. Standfuss, "Retinal isomerization in bacteriorhodopsin captured by a femtosecond X-ray laser," Science **361**(6398), eaat0094 (2018).

4. C. Milne, T. Schietinger, M. Aiba, A. Alarcon, J. Alex, A. Anghel, V. Arsov, C. Beard, P. Beaud, S. Bettoni, M. Bopp, H. Brands, M. Brönnimann, I. Brunnenkant, M. Calvi, A. Citterio, P. Craievich, M. Csatari Divall, M. Dällenbach, M. D'Amico, A. Dax, Y. Deng, A. Dietrich, R. Dinapoli, E. Divall, S. Dordevic, S. Ebner, C. Erny, H. Fitze, U. Flechsig, R. Follath, F. Frei, F. Gärtner, R. Ganter, T. Garvey, Z. Geng, I. Gorgisyan, C. Gough, A. Hauff, C. Hauri, N. Hiller, T. Humar, S. Hunziker, G. Ingold, R. Ischebeck, M. Janousch, P. Juranić, M. Jurcevic, M. Kaiser, B. Kalantari, R. Kalt, B. Keil, C. Kittel, G. Knopp, W. Koprek, H. Lemke, T. Lippuner, D. Llorente Sancho, F. Löhl, C. Lopez-Cuenca, F. Märki, F. Marcellini, G. Marinkovic, I. Martiel, R. Menzel, A. Mozzanica, K. Nass, G. Orlandi, C. Ozkan Loch, E. Panepucci, M. Paraliev, B. Patterson, B. Pedrini, M. Pedrozzi, P. Pollet, C. Pradervand, E. Prat, P. Radi, J.-Y. Raguin, S. Redford, J. Rehanek, J. Réhault, S. Reiche, M. Ringele, J. Rittmann, L. Rivkin, A. Romann, M. Ruat, C. Ruder, L. Sala, L. Schebacher, T. Schilcher, V. Schlott, T. Schmidt, B. Schmitt, X. Shi, M. Stadler, L. Stingelin, W. Sturzenegger, J. Szlachetko, D. Thattil, D. Treyer, A. Trisorio, W. Tron, S. Vetter, C. Vicario, D. Voulot, M. Wang, T. Zamofing, C. Zellweger, R. Zennaro, E. Zimoch, R. Abela, L. Patthey, and H.-H. Braun, "SwissFEL: The Swiss X-ray Free Electron Laser," Appl. Sci. **7**(7), 720 (2017).

5. R. Abela, P. Beaud, J. A. van Bokhoven, M. Chergui, T. Feurer, J. Haase, G. Ingold, S. L. Johnson, G. Knopp, H. Lemke, C. J. Milne, B. Pedrini, P. Radi, G. Schertler, J. Standfuss, U. Staub, and L. Patthey, "Perspective: Opportunities for ultrafast science at SwissFEL," Struct. Dyn. **4**(6), 061602 (2017).

6. J. M. Glownia, J. Cryan, J. Andreasson, A. Belkacem, N. Berrah, C. I. Blaga, C. Bostedt, J. Bozek, L. F. DiMauro, L. Fang, J. Frisch, O. Gessner, M. Gühr, J. Hajdu, M. P. Hertlein, M. Hoener, G. Huang, O. Kornilov, J. P. Marangos, A. M. March, B. K. McFarland, H. Merdji, V. S. Petrovic, C. Raman, D. Ray, D. A. Reis, M. Trigo, J. L. White, W. White, R. Wilcox, L. Young, R. N. Coffee, and P. H. Bucksbaum, "Time-resolved pump-probe experiments at the LCLS," Opt. Express **18**(17), 17620 (2010).

7. S. Schulz, I. Grguraš, C. Behrens, H. Bromberger, J. T. Costello, M. K. Czwalinna, M. Felber, M. C. Hoffmann, M. Ilchen, H. Y. Liu, T. Mazza, M. Meyer, S. Pfeiffer, P. Prędki, S. Schefer, C. Schmidt, U. Wegner, H. Schlarb, and A. L. Cavalieri, "Femtosecond all-optical synchronization of an X-ray free-electron laser," Nat. Commun. **6**(1), 5938 (2015).

8. M. Harmand, R. Coffee, M. R. Bionta, M. Chollet, D. French, D. Zhu, D. M. Fritz, H. T. Lemke, N. Medvedev, B. Ziaja, S. Toleikis, and M. Cammarata, "Achieving few-femtosecond time-sorting at hard X-ray free-electron lasers," Nat. Photonics **7**(3), 215–218 (2013).

9. M. Beye, O. Krupin, G. Hays, A. H. Reid, D. Rupp, S. de Jong, S. Lee, W.-S. Lee, Y.-D. Chuang, R. Coffee, J. P. Cryan, J. M. Glownia, A. Föhlisch, M. R. Holmes, A. R. Fry, W. E. White, C. Bostedt, A. O. Scherz, H. A. Durr, and W. F. Schlotter, "X-ray pulse preserving single-shot optical cross-correlation method for improved experimental temporal resolution," Appl. Phys. Lett. **100**(12), 121108 (2012).

10. S. Schorb, T. Gorkhover, J. P. Cryan, J. M. Glownia, M. R. Bionta, R. N. Coffee, B. Erk, R. Boll, C. Schmidt, D. Rolles, A. Rudenko, A. Rouzee, M. Swiggers, S. Carron, J.-C. Castagna, J. D. Bozek, M. Messerschmidt, W. F. Schlotter, and C. Bostedt, "X-ray–optical cross-correlator for gas-phase experiments at the Linac Coherent Light Source free-electron laser," Appl. Phys. Lett. **100**(12), 121107 (2012).

11. N. Hartmann, W. Helml, A. Galler, M. R. Bionta, J. Grünert, S. L. Molodtsov, K. R. Ferguson, S. Schorb, M. L. Swiggers, S. Carron, C. Bostedt, J.-C. Castagna, J. Bozek, J. M. Glownia, D. J. Kane, A. R. Fry, W. E. White, C. P. Hauri, T. Feurer, and R. N. Coffee, "Sub-femtosecond precision measurement of relative X-ray arrival time for free-electron lasers," Nat. Photonics **8**(9), 706–709 (2014).

12. W. Helml, I. Grguraš, P. Juranić, S. Düsterer, T. Mazza, A. Maier, N. Hartmann, M. Ilchen, G. Hartmann, L. Patthey, C. Callegari, J. Costello, M. Meyer, R. Coffee, A. Cavalieri, and R. Kienberger, "Ultrashort Free-Electron Laser X-ray Pulses," Appl. Sci. **7**(9), 915 (2017).

13. M. R. Bionta, N. Hartmann, M. Weaver, D. French, D. J. Nicholson, J. P. Cryan, J. M. Glownia, K. Baker, C. Bostedt, M. Chollet, Y. Ding, D. M. Fritz, A. R. Fry, D. J. Kane, J. Krzywinski, H. T. Lemke, M. Messerschmidt, S. Schorb, D. Zhu, W. E. White, and R. N. Coffee, "Spectral encoding method for measuring the relative arrival time between X-ray/optical pulses," Rev. Sci. Instrum. **85**(8), 083116 (2014).

14. O. Krupin, M. Trigo, W. F. Schlotter, M. Beye, F. Sorgenfrei, J. J. Turner, D. A. Reis, N. Gerken, S. Lee, W. S. Lee, G. Hays, Y. Acremann, B. Abbey, R. Coffee, M. Messerschmidt, S. P. Hau-Riege, G. Lapertot, J. Lüning, P. Heimann, R. Soufli, M. Fernández-Perea, M. Rowen, M. Holmes, S. L. Molodtsov, A. Föhlisch, and W. Wurth, "Temporal cross-correlation of X-ray free electron and optical lasers using soft X-ray pulse induced transient reflectivity," Opt. Express **20**(10), 11396 (2012).

15. M. R. Bionta, H. T. Lemke, J. P. Cryan, J. M. Glownia, C. Bostedt, M. Cammarata, J.-C. Castagna, Y. Ding, D. M. Fritz, A. R. Fry, J. Krzywinski, M. Messerschmidt, S. Schorb, M. L. Swiggers, and R. N. Coffee, "Spectral encoding of X-ray/optical relative delay," Opt. Express **19**(22), 21855 (2011).

16. T. Maltezopoulos, S. Cunovic, M. Wieland, M. Beye, A. Azima, H. Redlin, M. Krikunova, R. Kalms, U. Frühling, F. Budzyn, W. Wurth, A. Föhlisch, and M. Drescher, "Single-shot timing measurement of extreme-ultraviolet free-electron laser pulses," New J. Phys. **10**(3), 033026 (2008).

17. U. Frühling, M. Wieland, M. Gensch, T. Gebert, B. Schütte, M. Krikunova, R. Kalms, F. Budzyn, O. Grimm, J. Rossbach, E. Plönjes, and M. Drescher, "Single-shot terahertz-field-driven X-ray streak camera," Nat. Photonics **3**(9), 523–528 (2009).

18. B. Ziaja, R. A. London, and J. Hajdu, "Unified model of secondary electron cascades in diamond," J. Appl. Phys. **97**(6), 064905 (2005).

19. K. Mecseki, H. Höppner, M. Büscher, V. Tkachenko, N. Medvedev, J. J. Bekx, V. Lipp, P. Piekarz, M. Windeler, J. W. G. Tisch, D. J. Walke, M. Nakatsutsumi, M. J. Prandolini, J. M. Glownia, T. Sato, M. Sikorski, M. Chollet, U. Teubner, J. Robinson, S. Toleikis, B. Ziaja, and F. Tavella, "Hard X-ray induced fast secondary electron cascading processes in solids," Appl. Phys. Lett. **113**(11), 114102 (2018).

20. G. Ingold, R. Abela, C. Arrell, P. Beaud, P. Böhler, M. Cammarata, Y. Deng, C. Erny, V. Esposito, U. Flechsig, R. Follath, C. Hauri, S. Johnson, P. Juranic, G. F. Mancini, R. Mankowsky, A. Mozzanica, R. A. Oggenfuss, B. D. Patterson, L. Patthey, B. Pedrini, J. Rittmann, L. Sala, M. Savoini, C. Svetina, T. Zamofing, S. Zerdane, and H. T. Lemke, "Experimental station Bernina at SwissFEL: condensed matter physics on femtosecond time scales investigated by X-ray diffraction and spectroscopic methods," J. Synchrotron Radiat. **26**(3), 874–886 (2019).

21. C. Erny and C. P. Hauri, "The SwissFEL Experimental Laser facility," J. Synchrotron Radiat. **23**(5), 1143–1150 (2016).

22. R. W. Boyd, *Nonlinear Optics* (Academic Press, 2003).

23. O. Svelto, *Principles of Lasers* (Springer US, 2010).

24. R. A. Smith, *Semiconductors* (Cambridge University Press, 1978).

25. B. L. Henke, E. M. Gullikson, and J. C. Davis, "X-Ray Interactions: Photoabsorption, Scattering, Transmission, and Reflection at E = 50-30,000 eV, Z = 1-92," At. Data Nucl. Data Tables **54**(2), 181–342 (1993).

26. U. Teubner, U. Wagner, and E. Förster, "Sub-10 fs gating of optical pulses," J. Phys. B: At., Mol. Opt. Phys. **34**(15), 2993–3002 (2001).

27. R. Riedel, A. Al-Shemmary, M. Gensch, T. Golz, M. Harmand, N. Medvedev, M. J. Prandolini, K. Sokolowski-Tinten, S. Toleikis, U. Wegner, B. Ziaja, N. Stojanovic, and F. Tavella, "Single-shot pulse duration monitor for extreme ultraviolet and X-ray free-electron lasers," Nat. Commun. **4**(1), 1731 (2013).